Protein Science (1994), *3*:799–809. Cambridge University Press. Printed in the USA.

Structure of glutathione reductase from *Escherichia coli* at 1.86 Å resolution: Comparison with the enzyme from human erythrocytes

PEER R.E. MITTL AND GEORG E. SCHULZ

Institut für Organische Chemie und Biochemie, Albert-Ludwigs-Universität, 79104 Freiburg im Breisgau, Germany

(RECEIVED January 11, 1994; ACCEPTED March 3, 1994)

Abstract

The crystal structure of the dimeric flavoenzyme glutathione reductase from *Escherichia coli* was determined and refined to an *R*-factor of 16.8% at 1.86 Å resolution. The molecular 2-fold axis of the dimer is local but very close to a possible crystallographic 2-fold axis; the slight asymmetry could be rationalized from the packing contacts. The 2 crystallographically independent subunits of the dimer are virtually identical, yielding no structural clue on possible cooperativity. The structure was compared with the well-known structure of the homologous enzyme from human erythrocytes with 52% sequence identity. Significant differences were found at the dimer interface, where the human enzyme has a disulfide bridge, whereas the *E. coli* enzyme has an antiparallel β-sheet connecting the subunits. The differences at the glutathione binding site and in particular a deformation caused by a Leu–Ile exchange indicate why the *E. coli* enzyme accepts trypanothione much better than the human enzyme. The reported structure provides a frame for explaining numerous published engineering results in detail and for guiding further ones.

Keywords: asymmetries; crystal packing contacts; crystal structure; disulfide oxidoreductases; glutathione; trypanothione

Glutathione reductase (EC 1.6.4.2) catalyzes the reduction of oxidized glutathione according to: GSSG + NADPH + H^+ ⇄ 2GSH + $NADP^+$. The enzyme is important in maintaining a reducing environment within the cell (Akerboom et al., 1982); glutathione is involved in various cellular functions (Meister, 1989). Glutathione reductase from *Escherichia coli* is a homodimer with 450 amino acid residues and 1 FAD per subunit (M_r 49,560). It belongs to the family of FAD-dependent disulfide oxidoreductases, which also includes lipoamide dehydrogenase (Mattevi et al., 1991), trypanothione reductase (Kuriyan et al., 1991a), mercuric ion reductase (Schiering et al., 1991), and thioredoxin reductase (Kuriyan et al., 1991b).

The structure of glutathione reductase from human erythrocytes is known in great detail (Karplus & Schulz, 1987, 1989) and served as a guide for the design of several site-directed mutagenesis experiments on the enzyme GR_{eco}. Among them were the insertion of an intersubunit disulfide bridge (Scrutton et al., 1988), the identification of catalytically important residues (Deonarain et al., 1989; Scrutton et al., 1990a, 1992), the switch of the coenzyme specificity from NADP to NAD (Scrutton et al., 1990b), and the specificity change from glutathione to trypanothione (Henderson et al., 1991) and the reverse (Sullivan et al., 1991). Because the 2 enzyme species have only 52% amino acid residues in common (Greer & Perham, 1986), understanding the engineering results on the GR_{eco} necessitates detailed structural knowledge of this enzyme. We therefore established an accurate model by pursuing the structure analysis of GR_{eco} from the reported medium-resolution model (Ermler & Schulz, 1991) to high resolution.

Reprint requests to: Georg E. Schulz, Institut für Organische Chemie und Biochemie, Albertstr. 21, 79104 Freiburg im Breisgau, Germany; e-mail: schulz@bio2.chemie.uni-freiburg.de.

Abbreviations: B-factor, crystallographic temperature factor; GR_{eco}, glutathione reductase from *Escherichia coli*; GR_{hum}, human glutathione reductase; GSSG, oxidized glutathione; NCS, noncrystallographic symmetry; *R*-factor, crystallographic reliability factor; σ, standard deviation; MIR, multiple isomorphous replacement.

Results and discussion

Noncrystallographic symmetry

The diffraction pattern of the analyzed monoclinic form-P crystals at resolutions below 12 Å indicates a parent space group B2 with 1 subunit per asymmetric unit, which reveals the general crystal packing scheme. At higher resolution, however, the diffraction pattern corresponds either to space group $P2_1$ or to P2 with 2 subunits per asymmetric unit. With their medium-resolution data, Ermler and Schulz (1991) assumed space group

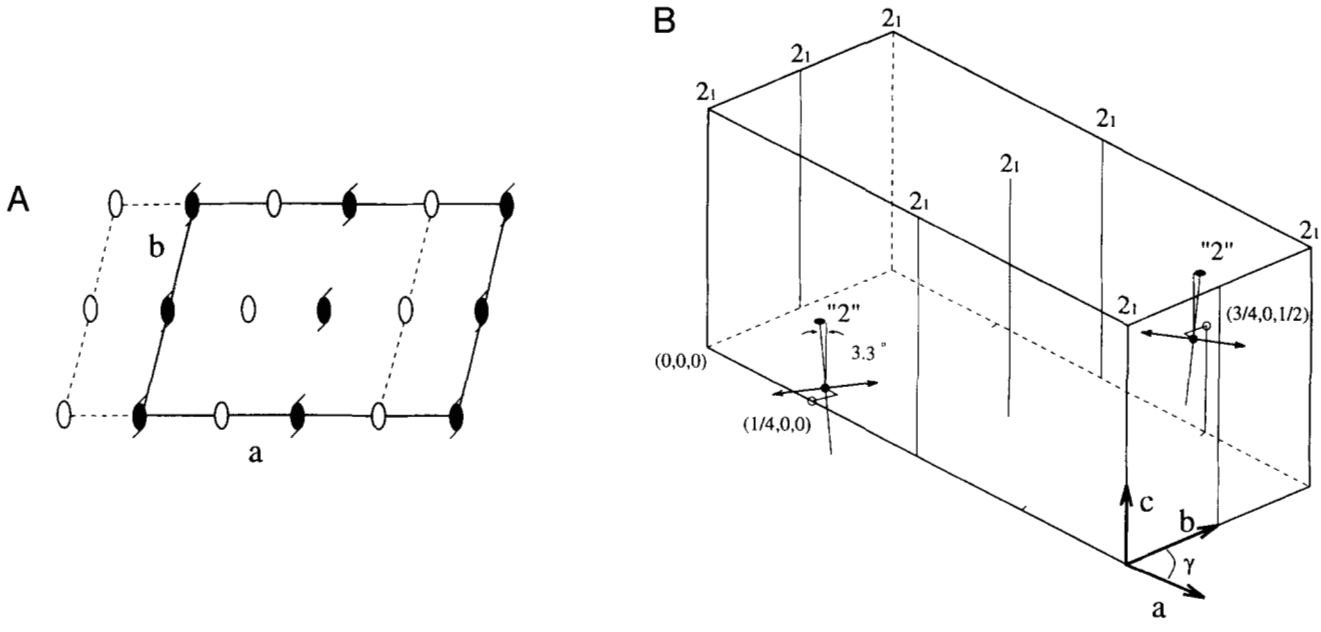

Fig. 1. Noncrystallographic symmetry in crystal form-P. **A:** Symmetry elements of parent space group B2 in 1 unit cell (dashed line). Breaking the 2-fold axes yields the actual space group $P2_1$ with shifted origin (solid line), whereas breaking of the screw axes leads to space group P2 that was assumed by Ermler and Schulz (1991) at medium resolution. **B:** Packing of enzyme molecules. The enzyme is a dimer of subunits I and II, which are represented as arrows. The molecular 2-fold axis ("2") is local in the crystal. The unit cell is defined by the 2_1-axes (parallel to the *c*-axis) and contains 2 dimers. As indicated by thin lines, the dimer centers of mass differ slightly from position (1/4, 0, 0) and its equivalent (3/4, 0, 1/2), which would be assumed in the parent space group B2. At (1/4, 0, 0) the displacement (Å) is (−0.1, 0.2, 0.0) and the molecular 2-fold axis ("2") has directional cosinus of (−0.046, 0.034, 0.988), giving rise to a tilt angle of 3.3°. The centers of mass of subunits I and II (Å) are at (19.1, 14.9, −0.9) and (40.9, −14.5, +0.9), respectively. Accordingly, the relative shift of the 2 crystallographically independent subunits along the *c*-axis is about 1.8 Å, which compares well with the 1.7 Å obtained by Ermler and Schulz (1991). The 0.4° rotational difference between dimers specified by Ermler and Schulz is within the limits of error of the earlier and of the present model.

P2 (destruction of the 2_1-axes of B2; Fig. 1A) because the intensity measurements of the 00*l* reflection row failed to indicate a 2_1-axis decisively. Starting from a model of the homologous GR_{hum} (Karplus & Schulz, 1987), the structural refinement of GR_{eco} in space group P2 reached an *R*-factor of 29.4% at 3 Å resolution.

With advanced equipment and larger and more numerous crystals, we now obtained more accurate data showing more clearly the systematic absences in the 00*l* row. Thus, we opted for the alternative space group $P2_1$ (destruction of the 2-axes of B2; Fig. 1A), in which the *R*-factor eventually ran down to 16.8% in the resolution range 7–1.86 Å, confirming this assignment. The crystal packing is illustrated in Figure 1B. The unit cell is defined by the 2_1-axes and contains 2 dimeric enzyme molecules with centers of mass close to (1/4, 0, 0) and (3/4, 0, 1/2), respectively. The molecular 2-fold axis is local, slightly tilted against the 2_1-axes, and slightly displaced from the center between 2_1-axes. Without tilt and shift, the local axis would be crystallographic, giving rise to the parent space group B2.

The known structure now allows a discussion of the earlier model. In their interpretation, Ermler and Schulz (1991) assumed space group P2 with true 2-axes and pseudo 2_1-axes. The 2_1-axes were broken by a relative dimer displacement of 1.7 Å along and a rotation of 0.4° around the *c*-axis. In spite of the wrong space group, the molecular replacement analysis (supported by low-resolution MIR data) yielded a seemingly reasonable model. A best superposition of single subunits of the early (Ermler & Schulz, 1991) and the present model of GR_{eco} resulted in an average RMS ΔC_α of 1.4 Å for the 4 pairwise subunit comparisons. This has to be related to the values for the subunit comparisons within each model, which were 0.38 Å (early model) and 0.27 Å (present model). Obviously, the refinement in the wrong space group at medium resolution had appreciably deformed the early model, although this model had been kept close to standard geometry (RMS deviations of bond lengths and angles of 0.027 Å and 5°).

Chain conformation

Following GR_{hum}, we divided the structure of GR_{eco} into 3 separate domains: the FAD domain (positions 1–140, 265–336), the NADP domain (positions 141–264), and the INTERFACE domain (positions 337–450). The NADP domain originated from a gene duplication of the FAD domain (Schulz, 1980). It should be mentioned that the domain definition of GR_{hum} has changed over time. The former definition of a CENTRAL domain, which had been introduced in order to have all domains consecutive along the chain, has been abandoned in view of the realization that there do exist domains inserted into other domains (Schulz, 1992). A Ramachandran plot for both independent subunits shows that most of the non-glycine residues cluster in the α-helical and β-sheet regions (Fig. 2). Nine non-glycine residues are in the

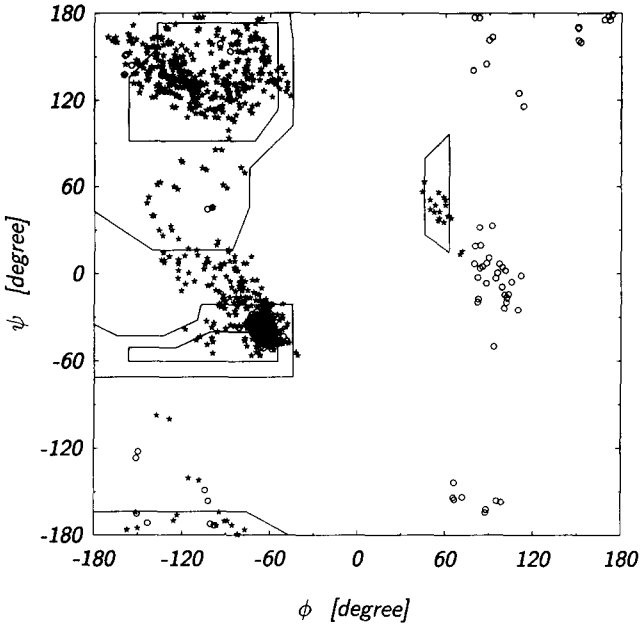

Fig. 2. Scatter plots of the main-chain torsion angles (ϕ, ψ) for all non-glycine (★) and glycine (○) residues from both subunits. The available conformational space for non-glycine residues is indicated by continuous lines. Outside these regions are Lys 36 and Lys 199 (see text). The RMS (ϕ, ψ) difference between subunits I and II is (2.8°, 2.5°) for non-glycines and (3.2°, 3.6°) for glycines.

Table 1. *Polar interactions between FAD and polypeptide chain*

FAD	GR_{eco}[a]		GR_{hum}[b]	
Atom 1	Atom 2	Distance (Å)	Atom 2	Distance (Å)
N1A	Ala 115-N	3.09 (3.05)	Ala 130-N	2.90
N3A	Ala 35-N	2.95 (2.99)	Ser 51-N	3.13
			Ser 51-OG	3.33
N6αA	Ala 115-O	3.02 (3.06)	Ala 130-O	3.08
O2'A	Glu 34-OE2	2.68 (2.80)	Glu 50-OE2	2.65
O3'A	Glu 34-OE1	2.75 (2.75)	Glu 50-OE1	2.69
OA1	Thr 41-OG1	2.71 (2.62)	Thr 57-OG1	2.85
OA2	Thr 41-N	2.92 (2.89)	Thr 57-N	3.16
	FAD-O4'F[c]	2.85 (2.64)	FAD-O4'F[c]	2.96
OF1	Gly 15-N	2.71 (2.84)	Gly 31-N	2.74
OF2	Asp 303-N	2.96 (2.89)	Asp 331-N	2.97
O3'F	Asp 303-OD2	2.75 (2.83)	Asp 331-OD2	2.76
O2'F	FAD-O4'F[c]	2.66 (2.80)	FAD-O4'F[c]	2.65
N1F	Thr 311-N	3.49 (3.44)	Thr 339-N	3.49
O2αF	Thr 311-N	3.07 (3.08)	Thr 339-N	3.10
N3F	His 439'-O	2.77 (2.73)	His 467'-O	2.74
O4αF	Lys 50-NZ	2.86 (2.74)	Lys 66-NZ	2.78
N5F	Lys 50-NZ	2.96 (3.07)	Lys 66-NZ	3.01
N10F	Tyr 177-OH	3.10 (3.11)	Tyr 197-OH	3.15

[a] The distances in parentheses refer to subunit II.
[b] Distances according to Karplus and Schulz (1987).
[c] Interactions within the FAD molecule.

left-handed α-helix region (60°, 40°). As to be expected (Matthews, 1977), 6 of them are asparagines.

In both subunits Lys 36 and Lys 199 have unfavorable (ϕ, ψ) angles around (−130°, −100°) and (−110°, −140°), respectively (Fig. 2), but well-defined densities. Lys 36 is equivalent to His 52 of GR_{hum}, which adopts the same unusual conformation. The peptide nitrogen of Lys 36 donates a hydrogen bond to the carboxylate of Glu 34, which in turn binds tightly to both hydroxyls of the adenine ribose of FAD (Table 1) and to another peptide (Gly 12-N), all in most favorable geometry. Residues Gly 12, Glu 34, and Lys 36 are all in the first βαβ-unit of the strongly conserved Rossmann fold for dinucleotide binding (Schulz, 1992).

Lys 199 in the NADP domain is equivalent to Lys 36 of the FAD domain, i.e., it is at the equivalent Rossmann fold position. Its main-chain conformation is unfavorable, although there is no hydrogen bond to a neighboring glutamate side chain because the equivalent residue is a valine (Val 197). Conceivably, the main-chain distortion bringing the carboxylate in good hydrogen bond geometry between 2 peptide nitrogens is required for adenosine binding and has been kept during the gene duplication, leading to the ancient NAD-binding lipoamide dehydrogenase. When the evolution proceeded to the more recent glutathione reductase, the glutamate was replaced by a valine in order to exclude adenosine ribose and thus NAD binding but promote NADP binding. Still, the chain fold was kept, and the distortion at Lys 199 remained as a rudiment.

There are 3 *cis*-peptides in GR_{eco} occurring before Pro 223, Pro 347, and Pro 440. Pro 347 and Pro 440 are also *cis*-prolines in GR_{hum} and they are conserved in the glutathione reductase from *Pseudomonas aeruginosa*, whereas Pro 223 is found exclusively in GR_{eco}. Pro 347 is in a tight reverse turn of the antiparallel β-sheet of the INTERFACE domain. The *cis*-peptide of Pro 440 is stabilized by 2 strong hydrogen bonds with the other subunit (His 439'-O···FAD-N3F and Pro 440-O···Lys 51'-NZ; Table 2). Pro 223 is close to Pro 347 in the loop between α-helix H6 and β-strand c3 (Figs. 3, 4).

Scatter plots of leucine and isoleucine side-chain torsion angles show that all (χ_1,χ_2) angles are within the regions for staggered conformation. Isoleucines assume predominantly (71%) the g^-t conformation, whereas leucines are evenly distributed over g^-g^- (52%) and tt (48%). All conformations are identical in both subunits except for Ile 230, which is close to crystal contact V (see below). Both Ile 20 have less favorable χ_1 angles, but are in well-defined densities.

The secondary structure assignment depends on the applied hydrogen bond criteria. Here, we used program DSSP (Kabsch & Sander, 1983). The results are given in Figure 3 together with a structure-based sequence alignment of GR_{eco} and GR_{hum}. The largest difference between GR_{eco} and GR_{hum} occurs around position 75, where GR_{eco} has the antiparallel intersubunit β-sheet g, whereas GR_{hum} has an intersubunit disulfide bridge (Cys 90··· Cys 90'). The chain-fold topology of GR_{eco} is sketched in Figure 4.

Chain mobility

The *B*-factor plots of both main chains (Fig. 5) resemble each other closely, although no noncrystallographic symmetry restraints were applied in the last 5 refinement rounds. Highest mobilities with *B*-factors above 40 Å^2 are found around positions 127 and 238 at the first loops in the β-meanders of the FAD

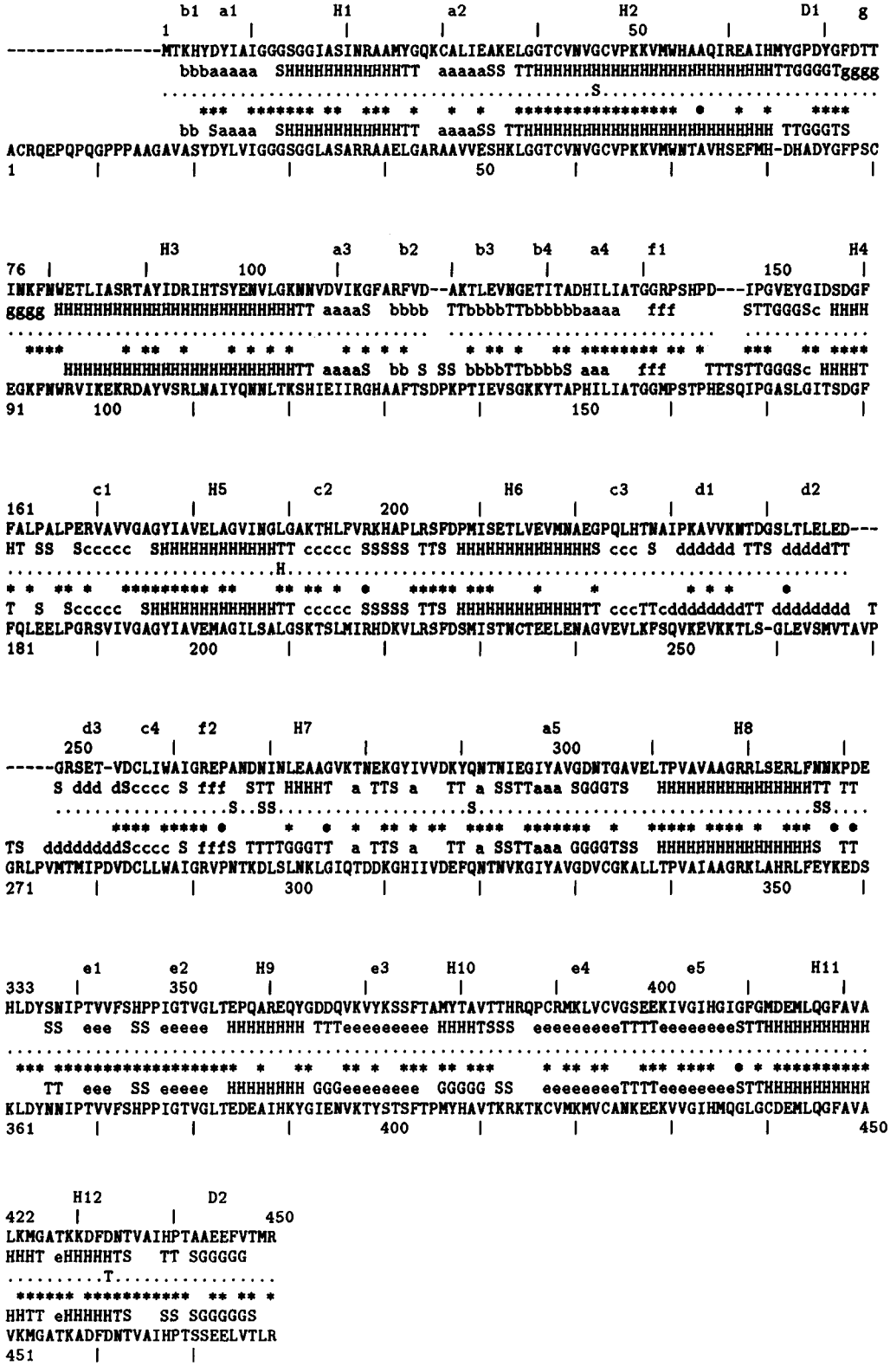

Fig. 3. Secondary structure assignment for GR_{eco} and GR_{hum} (Karplus & Schulz, 1987) using program DSSP (Kabsch & Sander, 1983; nomenclature: G, 3_{10}-helix; H, α-helix; S, bend; T, isolated turn with a hydrogen bond; a, b, c, d, e, f, g, β-strands named by β-sheet). The 5 assignments of single β-sheet residues denote very short strands that are not introduced in Figure 4. Line 1, secondary structures as depicted in Figure 4 (a1 . . . are β-strands, H1 . . . are α-helices, and D1 and D2 are 3_{10}-helices); lines 2 and 3, numbering and sequence of GR_{eco}; line 4, secondary structure for GR_{eco} subunit I; line 5, secondary structure of GR_{eco} subunit II with dots for elements identical to subunit I; line 6, sequence identity with GR_{hum} indicated by stars; lines 7, 8, and 9, secondary structure, sequence, and numbering of GR_{hum}.

Table 2. *Hydrogen bonds across the subunit interface*[a]

GR_{eco}			GR_{hum}[b]		
Atom 1	Atom 2	Distance (Å)	Atom 1	Atom 2	Distance (Å)
Lys 51-NZ	Pro 440-O	2.75 (2.71)	eq	eq	2.83
Glu 414-OE1	Ala 442-N	2.95 (3.03)	eq	Ser 470-N	2.96
Glu 414-OE2	Ala 443-N	2.95 (2.93)	eq	Ser 471-N	2.87
Gln 417-OE1	Ile 438-N	2.94 (2.87)	eq	eq	3.01
Gln 417-NE2	Val 436-O	3.12 (3.00)	eq	eq	3.03
–	–	–	Lys 452-NZ	Asn 462-O	2.85
FAD-N3F	His 439-O	2.77 (2.75)	eq	eq	2.74
Asp 69-O	Ser 87-OG	2.98 (3.04)	eq	Lys 102-NZ	2.91
Gly 71-O	Asn 80-N	2.70 (2.76)	eq	eq	2.72
Asp 73-N	Lys 78-O	2.88 (2.86)	–	–	–
Asp 73-O	Asn 77-N	2.60 (2.59)	–	–	–
Thr 75-N	Thr 75-O	2.80 (2.81)	–	–	–
Thr 75-OG	Asn 77-OD1	2.96 (3.14)	–	–	–
Arg 94-NH2	Ala 381-O	2.97 (3.48)	eq	eq	3.20
–	–	–	His 75-ND1	His 82-ND2	2.68

[a] Above the dotted line is the "upper" interface (segments 47–51, 312, 339–342, and 411–447) and below is the "lower" interface (segments 52–91 and 378–383).

[b] Taken from Karplus and Schulz (1987); eq means that the equivalent residue in GR_{hum} (Fig. 3) is identical.

and NADP domains, as well as around positions 268 and 330 of the FAD domain and around position 363 at the end of α-helix H9 in the INTERFACE domain.

The 2 FAD molecules are bound in a very rigid environment. As in GR_{hum}, there exists a *B*-factor gradient along FAD. The average *B*-factors of isoalloxazine, ribitol, pyrophosphate, adenine ribose, and adenine are 9.1 (7.9) Å^2, 11.9 (9.4) Å^2, 13.9 (10.0) Å^2, 16.3 (12.5) Å^2, and 22.9 (17.1) Å^2, where the values for subunit II are given in parentheses. This shows that the isoalloxazine has to be well fixed for the catalyzed electron transfer.

Solvent structure

The GR_{eco} model contains 645 water molecules with an average *B*-factor of 42 Å^2, all with densities above 1σ in the final $(2F_{obs} - F_{calc})$ map. The inner hydration shell of subunit I (dis-

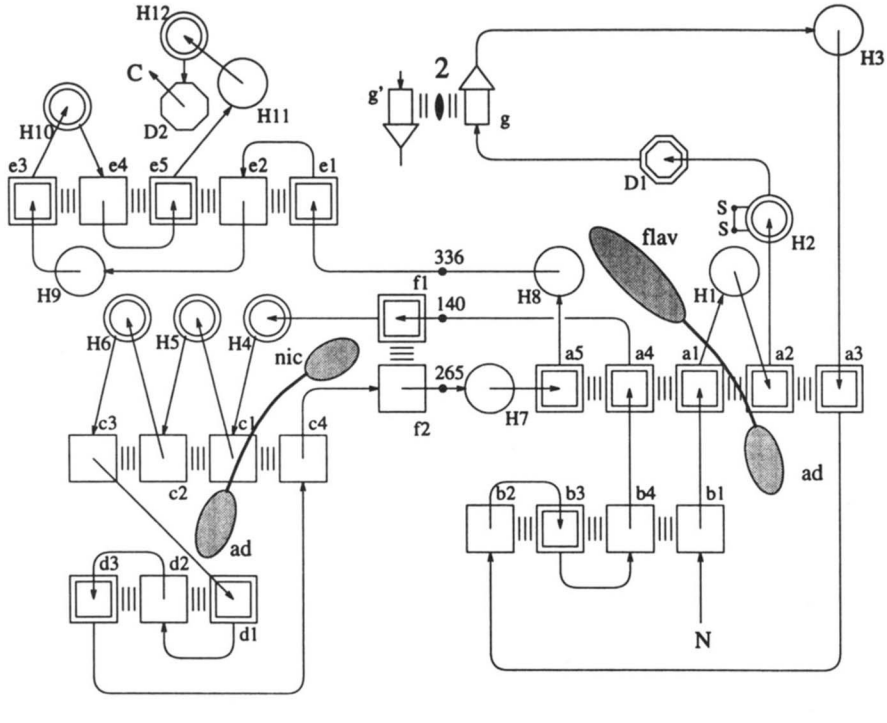

Fig. 4. Topology sketch of GR_{eco}. The view is approximately parallel to the molecular 2-fold axis. α-Helices are given as circles, 3_{10}-helices as octagons, and β-strands as squares. As an exception, the antiparallel intersubunit β-sheet (gg') is represented by arrows. Concentric symbols indicate that the chain runs into the paper plane. Hydrogen bonds within the β-sheets are indicated by 3 parallel lines. The domain borders are indicated by a dot and numbered. The bound FAD and NADP are sketched in gray. The domain names are obvious. The redoxactive disulfide is depicted.

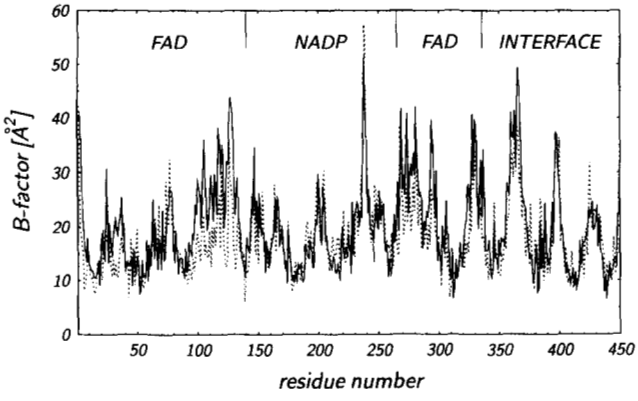

Fig. 5. Mobility along the polypeptide chain for subunit I (continuous line) and subunit II (dotted line) given as the average *B*-factor of the main-chain atoms of each residue. The average *B*-factor for all atoms including water molecules is 24.7 Å^2.

tance to a protein atom < 3.7 Å) contains 301 water molecules as compared to 307 in subunit II. The 37 water molecules of the second shell (3.7 Å ≤ distance < 4.5 Å) have an average *B*-factor of 57 Å^2, which is well above the general average. There are 64 pairs of water molecules that are superimposed within 1 Å by NCS. At 31 Å^2 the average *B*-factor of these pairs is significantly lower than the average.

A peculiar asymmetry occurs at Wat 367, which binds close to FAD and the redoxactive disulfide. In subunit I it forms extremely short hydrogen bonds with atoms FAD-OA2 (2.4 Å), FAD-O4'F (3.0 Å), Ser 14-OG (2.6 Å), and Gly 39-O (2.7 Å) and assumes a *B*-factor of 29 Å^2. At the equivalent position in subunit II, the $(F_{obs} - F_{calc})$ map shows positive density at 3 σ, but a water molecule at this position refines to less than 0.5σ electron density in the final $(2F_{obs} - F_{calc})$ map. GR_{hum} has a water molecule with full occupancy at the equivalent position.

Crystal contacts

GR_{eco} dimers form 5 crystal contacts to symmetry-related molecules (Table 3), among which the strongest interactions are at contact Ia and contact (IIa + IIb) with buried surface areas of 720 Å^2 and 690 Å^2, respectively. If the packing would follow exactly the parent space group B2 (Fig. 1), the contacts would be pairwise identical: I with II and III with IV, whereas V would have a 2-axis at its center. In the actual space group $P2_1$, these identities are reduced to similarities that can be visualized in Table 3 in the column specifying the involved residues. Here, lists *a*, *b*, *g*, *h*, and *k* resemble lists *c*, *d*, *i*, *j*, and *l*, respectively. Only lists *e* and *f* of contact IIb have no counterpart because the equivalent residues in the first contact are too far apart (shortest distance 7 Å), i.e., contact Ib is missing.

In the actual crystal, the symmetry-related contacts "I" and "II" of the parent space group B2 have become asymmetric after a small displacement, forming the superior contact Ia together with the small contact IIb at the expense of contact IIa (compare hydrogen bonds in Table 3). Presumably, a contact "Ia" (equal to "IIa") in parent space group B2 would be weak

Table 3. *Crystal contacts*

Contact	Buried area[a] (Å^2)	Contact[b] partners	Residues involved[c]	Polar interactions	Distance (Å)
Ia	720	$a{:}b_1$	*a*: 2′–6′, 25′–29′, 107′–109′, 326′–328′	Thr 2′-N···Ala 220-O	3.31
	720	$b{:}a_2$	*b*: 219–221, 384–386, 82′–101′	His 4′-N···Thr 384-O	2.82
				Asp 6′-OD2···Arg 386-NH1	2.81[d]
				Gly 27′-O···Arg 94′-NH1	2.90
				Asn 328′-ND2···Thr 97′-O	3.03
				Asn 328′-OD1···Asn 101′-ND2	3.01
IIa	535	$c{:}d_3$	*c*: 4–6, 25–28, 107, 326–328	Asp 6-OD1···Arg 386′-NH2	3.04[d]
	535	$d{:}c_4$	*d*: 82–97, 384′–386′	Gly 27-O···Arg 94-NH1	3.05
IIb	155	$e{:}f_3$	*e*: 366′–367′	Asn 126-O···Gln 367′-OE1	3.14
	155	$f{:}e_4$	*f*: 124–128		
III	150	$g{:}h_5$	*g*: 273–276		
	150	$h{:}g_6$	*h*: 149		
IV	135	$i{:}j_7$	*i*: 273′–274′		
	135	$j{:}i_8$	*j*: 149′		
V	235	$k{:}l_9$	*k*: 227–228, 248–250	Asn 228-ND2···Asp 248′-OD1	2.99
	235	$l{:}k_{10}$	*l*: 228′, 248′–250′	Arg 250-NH2···Asp 248′-O	3.23

[a] Accessible surface area of the reference molecule that is buried on crystallization as calculated with the program X-PLOR.

[b] Residue lists of reference molecule are *a*, *b*, . . . , whereas a_1, b_2, . . . are those of the neighbors. The crystallographically related molecules (1) through (10) are generated using the following rotations and translations (fractional coordinates): (1), S2 + (1, 0, 0); (2), S2 + (1, 0, −1); (3), S2; (4), S2 + (0, 0, −1); (5), S2 + (0, 1, 0); (6), S2 + (0, 1, −1); (7), S2 + (1, −1, 0); (8), S2 + (1, −1, −1); (9), S1 + (0, 1, 0); (10), S1 + (0, −1, 0); with S1 = identity, S2 = (−1, 0, 0|0, −1, 0|0, 0, 1) + (0, 0, 0.5).

[c] The residues belonging to subunit II are marked by a prime. For subunit definition see Figure 1.

[d] Salt bridge.

because of insufficient fit, and a contact "Ib" (equal to "IIb") in B2 would be very weak because of too large a distance. As a consequence, the observed slight asymmetry brings a large energy gain, which in turn rationalizes the actually assumed pseudosymmetry.

Whereas the large contacts Ia and (IIa + IIb) connect the dimers within the *a*,*c*-plane of the unit cell, the smaller contacts III, IV, and V are along the *b*-axis as the respective neighbor molecules (5) to (10) are shifted along *b* (Table 3). Contacts III and IV are weak because they contain only a nonpolar interaction involving a proline side chain and only indirect hydrogen bonds via water molecules. Despite this disparity between the 2 groups of contacts, however, the crystals grow to globular habits.

Altogether, the crystal contacts of a dimer cover an area of 3,860 Å^2, which is 13% of its solvent-accessible surface. For comparison, the packing contacts of GR_{hum} (without subunit interface) cover an area of 11% of its solvent-accessible surface area. Accordingly, GR_{eco} buries a larger fraction of its surface during crystallization than GR_{hum}.

Structural comparison between GR_{eco} and GR_{hum}

Because both structures are known at high resolution, a detailed comparison of GR_{eco} with the homologous enzyme GR_{hum} (52% identities) is of interest. The chain superposition results in 2 single-residue deletions in GR_{hum} at GR_{eco} position 65 in the "lower" part of the interface and at GR_{eco} position 240 in the first loop of a β-meander (Fig. 4). The additional residues of GR_{hum} are the 16-residue N-terminal extension, which is absent in all other known members of the enzyme family and invisible in the crystal structure, as well as 14 more residues after GR_{eco} positions 119, 147, 248, and 253. These additions are in the first loop of a β-meander, in the connecting segment between the FAD and NADP domains, as well as before and after the third strand of a β-meander (Fig. 3). Altogether, GR_{eco} is somewhat more compact than GR_{hum}.

The main-chain deviations between GR_{hum} and GR_{eco} are plotted in Figure 6; the RMS ΔC_α is 1.4 Å. Here, we superimposed the complete dimers in order to emphasize possible domain movements. The plots for subunits I and II of GR_{eco} are virtually identical because the RMS ΔC_α between the 2 independent subunits is only 0.27 Å. The 2 largest deviations occur at position 76, where β-sheet gg′ of GR_{eco} has been replaced by a disulfide in GR_{hum}, and at position 120, where GR_{hum} has an insertion in the first loop of a β-meander. As to be expected, the other peaks are generally at the surface.

Figure 6 shows different ΔC_α levels for the 3 domains, which prompted us to calculate the superpositions separately for each domain of subunit I of GR_{eco}. These calculations yielded RMS ΔC_α values of 1.3 Å, 1.0 Å, and 0.6 Å for the 208 C_α atoms of the FAD domain, the 123 C_α atoms of the NADP domain, and the 114 C_α atoms of the INTERFACE domain, respectively. Because these values are significantly smaller than the averages visually derived from Figure 6, we conclude that there are smallish domain movements between GR_{eco} and GR_{hum}, which went undetected at medium resolution (Ermler & Schulz, 1991). This is confirmed by a comparison of the transformation matrices for the single-domain superpositions, showing a 5° rotation angle between the FAD and INTERFACE domains.

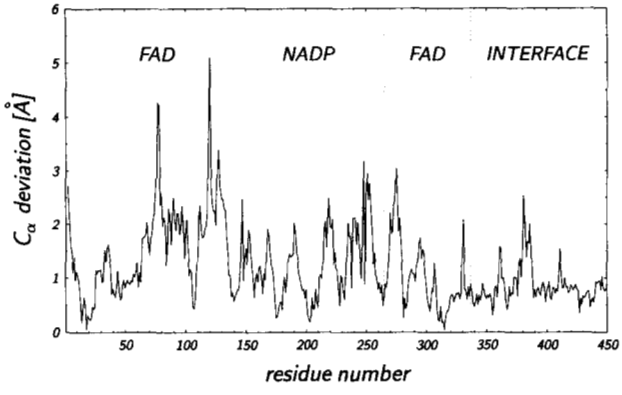

Fig. 6. Residual C_α distances between subunit I of GR_{eco} and GR_{hum} based on a best superposition of the 892 equivalent C_α atoms of the dimers. The numbering follows the GR_{eco} structure; the domains are indicated.

The FAD binding site of the enzyme is well conserved between GR_{eco} and GR_{hum}, in particular around the isoalloxazine moiety. This is explained by the importance of the isoalloxazine for catalysis (Karplus & Schulz, 1989). A best superposition of all FAD atoms results in an RMS deviation of only 0.14 Å (0.15 Å for subunit II), which corresponds to the error level. The direct polar interactions between FAD and polypeptide are listed in Table 1.

Two fingerprints for FAD binding have been reported: first, sequence Gly-X-Gly-X-X-Gly as a general motif for dinucleotide binding (see Schulz, 1992), and second, the special motif T-X-X-X-X-h-y-h-h-G-D, where h represents a small nonpolar residue and y an aromatic residue (Eggink et al., 1990). In GR_{eco} the general motif is Gly^{11}-Gly-Gly-Ser-Gly-Gly (completely conserved in GR_{hum}). It forms the first turn of helix H1 (Fig. 3) that stabilizes the pyrophosphate moiety of FAD by dipole interactions. The special motif is sequence Thr ^{293}-Asn-Ile-Glu-Gly-Ile-Tyr-Ala-Val-Gly-Asp (exchanges I295V and E296K in GR_{hum}), which contains strand a5 of the central β-sheet of the FAD domain, completing this sheet after the inserted NADP domain (Fig. 4). Obviously, these sequences are well conserved. Thr 293 stabilizes a loop by 2 strong hydrogen bonds from its OG1 atom to Ile 295-N and to Ile 298-O. Gly 302 adopts (ϕ,ψ) angles prohibited for non-glycines; moreover, a side chain would collide with the pyrophosphate of FAD. The carboxylate of Asp 303 forms a hydrogen bond to the ribitol moiety of FAD (Table 1).

As in GR_{hum}, the active center of GR_{eco} is distributed over both subunits, which are connected by a large interface, burying a solvent-accessible surface area of 3,600 Å^2 per subunit. This interface can be subdivided into a larger "upper" part with an area of 2,010 Å^2 and a smaller "lower" part with 1,590 Å^2 that are separated by a large internal cavity filled with water. The naming follows GR_{hum}. The hydrogen bonds across this interface are listed in Table 2. The larger "upper" part has fewer bonds than the smaller "lower" part, indicating that the "upper" interface is rather nonpolar. This nonpolar fit appears to be rather sensitive because it is strongly conserved. With 87% identical amino acids, the "upper" part is much more strongly conserved than the average of 52%, whereas the 48% conservation of the "lower" part is below average. An intersubunit disulfide

bridge in the "lower" interface is only known for GR_{hum}. The other dimeric disulfide-oxidoreductases (lipoamide dehydrogenase, trypanothione reductase, mercuric reductase) have a small antiparallel β-sheet similar to gg' of GR_{eco} (Fig. 4).

Figure 7 shows a superposition of this β-sheet gg' onto the GR_{hum} structure. Scrutton et al. (1988) produced the mutant Thr 75 → Cys of GR_{eco} designed to form the disulfide bridge of GR_{hum}. From the geometry of the Thr 75 side chain, it seems likely that the formation of the disulfide bridge disrupts the β-sheet. Probably this mutant has weakened the interface more than strengthened it.

There is some discussion of subunit cooperativity in oligomeric enzymes, which applies in particular for the dimeric glutathione reductase as its active centers are shared between subunits. Moreover, the introduction of a clear cooperativity by a point mutation at its subunit interface had been demonstrated by Scrutton et al. (1992). Subunit cooperativity implies conformational states that break the molecular symmetry, here the molecular 2-axis because, for instance, binding at one subunit should affect binding at the other. In the GR_{hum} structure, the molecular 2-axis is crystallographic, preventing the analysis of asymmetry. In contrast, the molecular 2-axis of GR_{eco} is local in the reported form-P crystal structure, which allows for the detection of asymmetric conformational states if there were any. Except for Wat 367 described above, no asymmetry of any importance could be found. Accordingly, the GR_{eco} structure cannot contribute much to the cooperativity discussion.

Active site

The active site of GR_{hum} has been analyzed in detail with and without substrate and substrate analogues (Karplus & Schulz, 1989; Janes & Schulz, 1990). Unfortunately, we did not succeed in binding GSSG to crystalline GR_{eco} so that we have to refer to the GSSG binding mode in GR_{hum} as depicted in the superposition of Figure 8. Among the 14 residues of GR_{hum} that contact GSSG directly or indirectly via water, there are only 2 exchanges in GR_{eco}, both of which concern residues involved in binding the glycine carboxylates of GSSG. These exchanges (Asn 21 of GR_{eco} vs. Arg 37 of GR_{hum} and Val 102 vs. Asn 117) diminish the binding strength of these carboxylates, which is already low in GR_{hum} (Janes & Schulz, 1990). This may be part of the reason why GR_{eco} shows an appreciable catalytic activity for trypanothione (N^1,N^8-bis(glutathionyl)spermidine) where these 2 carboxylates are amidated by a bridging spermidine (k_{cat}/K_M value around 1% of those of trypanothione reductases), whereas GR_{hum} has virtually none (Henderson et al., 1991).

Another, more subtle difference is the exchange Ile 95 of GR_{eco} vs. Leu 110 of GR_{hum}, which pushes the conserved Tyr 99 to about 2.5 Å away, deforming the main chain at this position. This displacement certainly modifies GSSG binding because Tyr 99 intercalates between the 2 cysteines and the 2 glycines of bound GSSG. This shift is likely to promote trypanothione activity because this isoleucine and a similarly displaced tyrosine side chain are also present in trypanothione reductase (Kuriyan et al., 1991a; Hunter et al., 1992). The broader substrate specificity of GR_{eco} may be correlated to the presence of glutathionyl spermidine in the stationary growth phase of *E. coli*. This metabolite may play a part in the control of growth and in nucleic acid metabolism (Tabor & Tabor, 1975).

The reported structure (Fig. 8) is consistent with engineering results on GR_{eco} that increased the catalytic rate for trypanothione (Henderson et al., 1991). They agree also with mutagenesis results on the homologous enzyme trypanothione reductase that increased its catalytic rate for GSSG (Sullivan et al., 1991).

Materials and methods

Purification and crystallization

Glutathione reductase was expressed in *E. coli* strain SG5 containing the gene on vector pKK223-3 and purified as described by Scrutton et al. (1987). Immediately before crystallization the enzyme was run through a final purification step. For this purpose 50 mg enzyme was loaded onto a 2',5'-ADP-Sepharose-4B affinity column (1.5 × 10 cm) and washed with 300 mL buffer

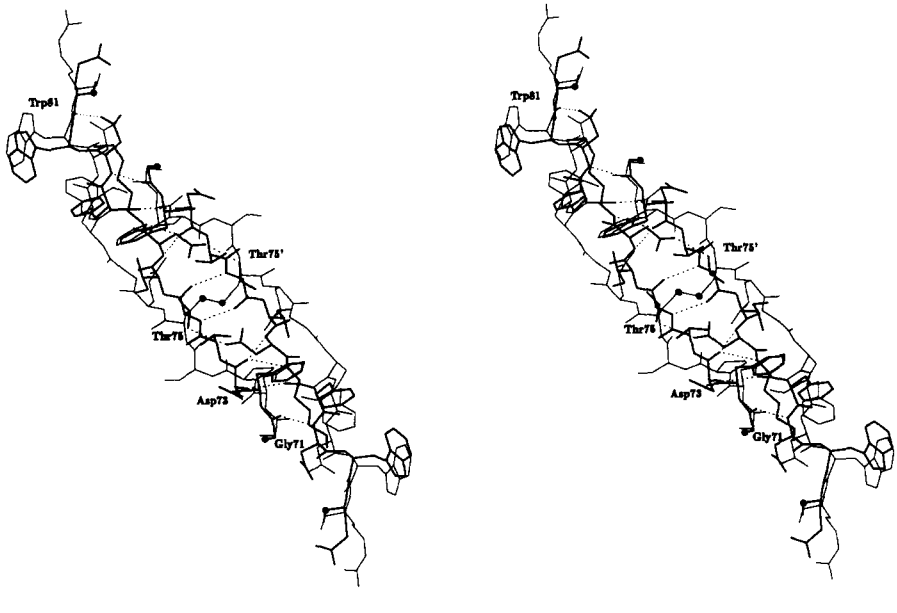

Fig. 7. Stereo view of a best superposition of the smaller "lower" part of the interface from GR_{eco} (thick line) onto GR_{hum} (thin line). The depicted segment contains residues 71–82 of GR_{eco} and residues 86–97 of GR_{hum}. The superposition is based on segment 66–86 (GR_{eco}). Hydrogen bonds in GR_{eco} are indicated by dashed lines. Chain cuts and the sulfurs of the disulfide bridge of GR_{hum} are marked by dots.

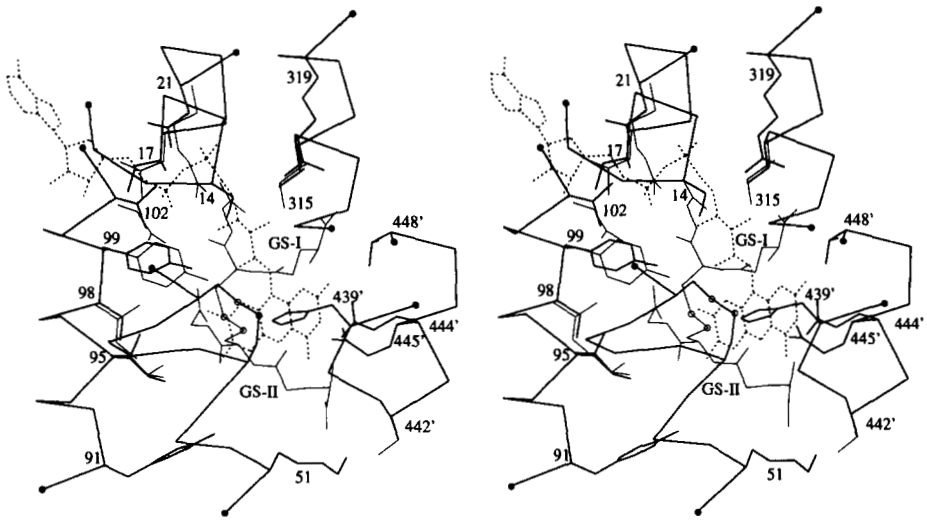

Fig. 8. Stereo view of the GSSG binding region of GR_{eco} (thick line) with its FAD (dashed line) as superimposed onto GR_{hum} with bound GSSG (thin line; Karplus & Schulz, 1989). Depicted is the C_α backbone of GR_{eco} (segments 11–22, 41–52, 90–103, 310–320, 438′–449′) together with essential side chains. These are Ser 14, Ile 17 (exchanged for Leu in GR_{hum}), Asn 21 (Arg), the redoxactive disulfide Cys 42–Cys 47, Lys 51, Tyr 91, Ile 95 (Leu), Ser 98 (Ile), Tyr 99, Val 102 (Asn), Val 315 (Ile), Arg 319, His 439′, Ala 442′ (Ser), Glu 444′, Glu 445′, and Thr 448′. The chain cuts are marked by dots and the sulfur atoms by circles. The superposition is based on local C_α atoms (segments 14–21, 39–51, 91–102, 378′, 439′–448′ of GR_{eco}).

A (20 mM potassium phosphate, pH 7.5, 1 mM EDTA) containing 180 mM KCl. The enzyme was eluted with 150 mL buffer A containing 500 mM KCl. Fractions with activities above 20 units/mL were pooled. After ultrafiltration, the final enzyme concentration was 30 mg/mL as based on $\epsilon_{460} = 11{,}300$ $M^{-1}\,cm^{-1}$ (oxidized flavin). The A_{280}/A_{460} ratio was 7.8. The protein was pure with respect to SDS-PAGE and isoelectric focusing. Its specific activity was 265 units/mg, which is somewhat lower than the 300 units/mg determined at the same conditions by Scrutton et al. (1987).

The enzyme crystallized at 20 °C in hanging drops yielding crystal forms-T and -P, both of which were suitable for X-ray analysis (Table 4). The crystallization conditions of these crystal forms are very similar, except for the source of the precipitant and the method of its application. Still, both forms could be produced separately and reproducibly. Crystal form-T (tetragonal) diffracted only to medium resolution. An attempt to improve these crystals by contact engineering shortened the crystallization time by a factor of 40, but failed to improve the resolution (Mittl et al., 1994). The superior crystal form-P had been reported by Ermler and Schulz (1991). It was now produced at slightly different conditions, yielding large-size crystals. We did not attempt to reproduce form-S crystals obtained with several salts by Ermler and Schulz (1991) because they had diffracted merely to medium resolution.

Data collection and structure determination

Native data of form-T crystals were collected on a 4-circle diffractometer (model $P2_1$, Nicolet/Siemens) as specified in Table 5. Native data of form-P crystals were collected on a 3-circle area detector (model X1000, Nicolet/Siemens) using Cu Kα radiation

Table 4. *Crystallization of glutathione reductase from E. coli*

	Form-T	Form-P
Reservoir	20 mM $K_xH_{3-x}PO_4$, pH 5.4, 20% PEG-10000[a]	100 mM $K_xH_{3-x}PO_4$, pH 5.5, 20% PEG-8000[a]
Drop	20 mM $K_xH_{3-x}PO_4$, pH 5.4, protein[b]: 16–22 mg/mL 5% PEG-10000, 0.02% NaN_3	100 mM $K_xH_{3-x}PO_4$, pH 5.5, protein[c]: 15–30 mg/mL 7% PEG-8000, 0.02% NaN_3
Seeding	None	Micro and macro
Duration	3–4 days	1 week
Size	$1{,}500 \cdot 300 \cdot 300\ \mu m^3$	$900 \cdot 500 \cdot 250\ \mu m^3$
Habit	Tetragonal bipyramid	Rectangular prism
Space group	$P4_32_12$	$P2_1$
Cell parameter	$a = b = 62$ Å, $c = 336.5$ Å	$a = 120.5$ Å, $b = 73.6$ Å, $c = 60.5$ Å, $\gamma = 83.0°$
Diffraction limit	3.0 Å	1.8 Å
Asymmetric unit	1 subunit	2 subunits
Solvent content	71%	54%

[a] PEG-10000 was from Fluka and PEG-8000 from Sigma.

[b] The enzyme solution (16–22 mg/mL, 100 μL) was dialyzed (Servapor membrane, exclusion limit 10–15 kDa) overnight at 4 °C against 100 mL 5% PEG-10000 in 20 mM $K_xH_{3-x}PO_4$, pH 5.4, 0.02% NaN_3. A drop was 5 μL of this solution. The average M_r of PEG in the drop is probably lower than 10,000.

[c] A 100-μL aliquot of enzyme solution (24–33 mg/mL) was dialyzed against 100 mL 100 mM $K_xH_{3-x}PO_4$, pH 5.5, 0.02% NaN_3. A drop contained 4 μL dialyzed and 2 μL reservoir solution.

from a rotating anode with graphite monochromator (model RU200B, Rigaku). Each data frame reported an angular range of 0.25° and was measured for 2 min. Data were processed with program XDS (Kabsch, 1988). The data from 3 GR_{eco} crystals were merged with program BIGNORD (Table 5).

One subunit of the GR_{eco} model of Ermler and Schulz (1991) served as a starting model for solving the structure of form-T crystals by molecular replacement. The cross-rotation function was calculated with program ALMN (SERC, 1979) using data between 12 and 4.6 Å resolution (Patterson radius 6–30 Å). The highest peak was at Eulerian angles $(\theta_1, \theta_2, \theta_3) = (135°, 90°, 330°)$; it was weak and only 1.6σ above the average. The 3-dimensional translation function calculated with program RSE3 (Diederichs & Schulz, 1990), using data between 15 and 9 Å, yielded sharp single peaks for the 2 possible space groups $P4_12_12$ and $P4_32_12$. The decision for $P4_32_12$ was based on an R_F-value of 46.5% (versus 55.2% for the alternative). Using program X-PLOR (Brünger et al., 1987), the model was then refined to an R-factor of 32.9% in the resolution range 9–3.1 Å at reasonable geometry (RMS deviations of bond lengths and angles are 0.03 Å and 5.4°). A best superposition with the 2 independent subunits of Ermler and Schulz (1991) showed an RMS ΔC_α of 0.9 Å for each comparison.

Subsequently, the crystal form-T model was used to solve the form-P crystal structure (Table 4) at high resolution. First we generated a symmetric dimer by a crystallographic rotation. Using this dimer as search molecule, the cross-rotation function of program ALMN (resolution 10–4.6 Å, Patterson radius 6–40 Å) yielded a clear solution with a 14σ peak at $(\theta_1, \theta_2, \theta_3) = (210°, 90°, 45°)$, the second highest peak being at 6σ. A following Patterson-correlation refinement (program suite X-PLOR) increased the correlation coefficient from 0.20 to 0.33 (resolution 10–6 Å, 15 cycles) and then from 0.15 to 0.31 (resolution 10–4 Å, 15 cycles). After that, a 2-dimensional translation function (resolution 10–4 Å) yielded a sharp 13σ peak at (0.25, 0.00, 0.00). The appropriately positioned search model had an R-factor of 53.5% in the resolution range 10–3 Å, which was reduced to 44.9% by 40 cycles of rigid-body refinement with separated subunits.

Structure refinement

The refinement was continued by simulated annealing using X-PLOR on a Cray-YMP8/832 (HLRZ-Jülich) and on an IBM-6000 workstation. The protocol of Brünger et al. (1987) was followed (Table 6). At the beginning of rounds 1–4, the B-factors were set uniformly to 15 Å^2 for protein and FAD atoms and to 35 Å^2 for water molecules. After each round the model was visually checked using $(2F_{obs} - F_{calc})\exp(i\alpha_{calc})$ and $(F_{obs} - F_{calc})\exp(i\alpha_{calc})$ electron density maps. The main errors of the model were in segment 228–250 of the β-meander in the NADP domain, in segments 62–79 and 306–310, and at the N-terminus. After round 1, the first 2 residues of each subunit were deleted because they caused strong negative density in the $(F_{obs} - F_{calc})$ map.

In rounds 1 and 2, NCS was enforced by applying a high NCS weight of 200 kcal·mol^{-1}. In rounds 3–7, the NCS weights were lowered to 10 kcal·mol^{-1} for main-chain atoms and to 5 kcal·mol^{-1} for side chains. No NCS restraints were applied for water molecules. Water molecules were only incorporated if their densities in the $(F_{obs} - F_{calc})$ map were above 3σ and their distances to protein atoms were in the range 2.3–4.5 Å. They were erased if their density in the $(2F_{obs} - F_{calc})$ map dropped below 1σ. After round 7, all NCS restraints were removed, and after round 8, all B-factor restraints were removed.

During the refinement, 2 alternate side-chain conformations of Cys 389 were found in both subunits and refined as such. Moreover, emerging electron density was assigned to Thr 2′ of subunit II, whereas Thr 2 of subunit I remained invisible. Thr 2′ participates in a crystal contact, whereas Thr 2 does not. The carboxamide orientations of Asn and Gln residues were assigned according to the B-factor differences between N and O atoms, minding possible hydrogen bonds. The imidazole side chains of His were oriented to form the maximum number of hydrogen bonds. At the end, all water molecules were renumbered according to their electron densities. The refinement resulted in an R-factor of 16.8% (Table 6) at good geometry. The RMS deviations from standard geometry were 0.016 Å and 2.8°.

Table 5. *Data collection statistics*

	Form-T crystals[a]	Form-P crystals[b]			
		No. 1	No. 2	No. 3	Merged
Resolution range (Å)	∞–3.0	∞–1.89	∞–1.86	∞–1.86	∞–1.86
Observations		190,063	216,430	162,505	
Unique reflections	14,133	67,438	70,516	67,715	83,086
R_{sym}[c] (%)	15.3[d]	5.8	5.2	5.9	9.1[e]
Completeness					
Total (%)	99.9	80.5	80.3	76.7	95.1
Outermost shell (%)		26.6	40.7	15.5	78.3

[a] Data were collected on a 4-circle diffractometer (model $P2_1$, Nicolet/Siemens).

[b] Data were collected on a 3-circle area detector (model X1000, Xentronics/Siemens).

[c] $R_{sym} = \sum_{i,hkl}|I(i,hkl) - \langle I(hkl)\rangle| / \sum_{i,hkl} I(i,hkl)$, where i runs through symmetry-related reflections.

[d] In this case R_{sym} is defined as: $R_{sym} = 2\sum|F_1 - F_2| / \sum(F_1 + F_2)$, where F_1 and F_2 are the structure factor amplitudes of the symmetry-related reflection zones $(hk1)$ and $(hk-1)$.

[e] Calculated in program BIGNORD.

Table 6. *Refinement results with X-PLOR*

Round	Resolution (Å)	R-factor[a] Begin (%)	R-factor[a] End (%)	RMS deviation Lengths (Å)	RMS deviation Angles (°)	Number of water molecules
1–4[b]	10–2.1	44.9	21.3	0.015	3.1	389
5–7	10–2.0	23.8	18.3	0.014	2.9	575
8–11	7–1.86	19.5	16.8	0.016	2.8	645

[a] The refinement protocol was: 80 cycles of conjugate gradient minimization (step-size $\Delta F = 0.2$ Å), 0.25 ps molecular dynamics at 300 K (timestep = 1 fs), 80 cycles of conjugate gradient minimization ($\Delta F = 0.005$ Å), 15 cycles of overall B-factor refinement, followed by 20 cycles of restrained individual B-factor refinement.

[b] In round 1, the "slowcool" protocol (Brünger et al., 1990) was run from 2,000 K to 800 K with $\Delta T = 50$ K (timestep = 0.5 fs, $\Delta F = 0.2$ Å) and from 800 K to 300 K with $\Delta T = 25$ K (timestep = 1 fs, $\Delta F = 0.2$ Å).

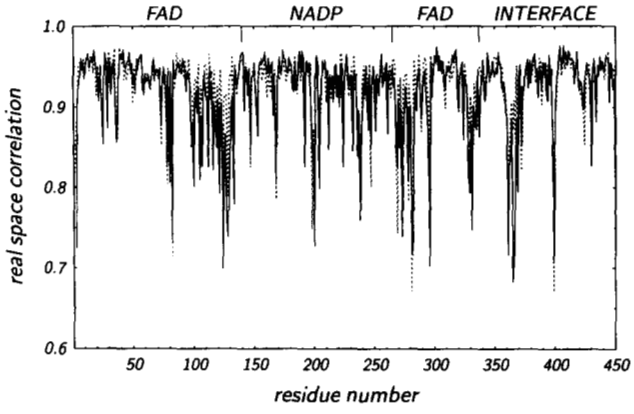

Fig. 9. Real-space correlation coefficient between observed and calculated electron densities along the main chains of subunit I (solid line) and subunit II (dashed line) according to Jones et al. (1991).

Quality of the model

The maximum coordinate error of the final GR_{eco} model was estimated to 0.2 Å according to a Luzzati plot (Luzzati, 1952). All atoms are in well-defined density as demonstrated by the real-space density fit shown in Figure 9 (Jones et al., 1991). In both subunits the densities for the side chains of Lys 78, Glu 82, His 200, Glu 281, Lys 282, Glu 399, Lys 430, and Arg 450 are missing. Because all these residues are located at the protein surface, they are likely to be highly mobile.

The coordinates and the structure factors of GR_{eco} are deposited in the Protein Data Bank at Brookhaven, New York.

Acknowledgments

The protein was produced and partly purified in the group of Dr. R.N. Perham in Cambridge, UK. We thank Dr. N.S. Scrutton and Dr. A. Berry for their kind support during protein purification at Cambridge.

References

Akerboom TPM, Bilzer M, Sies H. 1982. The relationship of biliary glutathione disulfide efflux and intracellular glutathione disulfide content in perfused rat liver. *J Biol Chem 257*:4248–4256.

Brünger AT, Krukowski J, Erickson J. 1990. Slow-cooling protocols for crystallographic refinement by simulated annealing. *Acta Crystallogr A 46*:585–593.

Brünger AT, Kuriyan J, Karplus M. 1987. Crystallographic *R*-factor refinement by molecular dynamics. *Science 235*:458–460.

Deonarain MP, Berry A, Scrutton NS, Perham RN. 1989. Alternative proton donors/acceptors in the catalytic mechanism of the glutathione reductase of *Escherichia coli*: The role of histidine-439 and tyrosine-99. *Biochemistry 28*:9602–9607.

Diederichs K, Schulz GE. 1990. Three-dimensional structure of the complex between the mitochondrial matrix adenylate kinase and its substrate AMP. *Biochemistry 29*:8138–8144.

Eggink G, Engel H, Vriend G, Terpstra P, Witholt B. 1990. Rubredoxin reductase of *Pseudomonas oleovorans*: Structural relationship to other flavoprotein oxidoreductases based on one NAD and two FAD fingerprints. *J Mol Biol 212*:135–142.

Ermler U, Schulz GE. 1991. The three-dimensional structure of glutathione reductase from *Escherichia coli* at 3 Å resolution. *Proteins Struct Funct Genet 9*:174–179.

Greer S, Perham RN. 1986. Glutathione reductase from *Escherichia coli*: Cloning and sequence analysis of the gene and relationship to other flavoprotein disulfide oxidoreductases. *Biochemistry 25*:2736–2742.

Henderson GB, Murgolo NJ, Kuriyan J, Osapay K, Kominos D, Berry A, Scrutton NS, Hinchliffe N, Perham RN, Cerami A. 1991. Engineering the substrate specificity of glutathione reductase toward that of trypanothione reduction. *Proc Natl Acad Sci USA 88*:8769–8773.

Hunter WN, Bailey S, Habash J, Harrop SJ, Helliwell JR, Aoagye-Kwarteng T, Smith K, Fairlamb AH. 1992. Active site of trypanothione reductase. *J Mol Biol 227*:322–333.

Janes W, Schulz GE. 1990. Role of charged groups of glutathione disulfide in the catalysis of glutathione reductase: Crystallographic and kinetic studies with synthetic analogues. *Biochemistry 29*:4022–4030.

Jones TA, Zou JY, Cowan SW, Kjeldgaard M. 1991. Improved methods for building protein models in electron density maps and the location of errors in these models. *Acta Crystallogr A 47*:110–119.

Kabsch WJ. 1988. Evaluation of single crystal X-ray diffraction data from a position-sensitive detector. *J Appl Crystallogr 21*:916–924.

Kabsch WJ, Sander C. 1983. Dictionary of protein secondary structure: Pattern recognition of hydrogen-bonded and geometrical features. *Biopolymers 22*:2577–2637.

Karplus PA, Schulz GE. 1987. Refined structure of glutathione reductase at 1.54 Å resolution. *J Mol Biol 195*:701–729.

Karplus PA, Schulz GE. 1989. Substrate binding and catalysis by glutathione reductase as derived from refined enzyme:substrate crystal structures at 2 Å resolution. *J Mol Biol 210*:163–180.

Kuriyan J, Kong XP, Krishna TSR, Sweet RM, Murgolo NJ, Field H, Cerami A, Henderson GB. 1991a. X-ray structure of trypanothione reductase from *Crithidia fasciculata* at 2.4 Å resolution. *Proc Natl Acad Sci USA 88*:6764–6768.

Kuriyan J, Krishna TSR, Wong L, Guenther B, Pahler A, Williams CH Jr, Model P. 1991b. Convergent evolution of similar function in two structurally divergent enzymes. *Nature (Lond) 352*:172–174.

Luzzati V. 1952. Traitement statistique des erreurs dans la determination des structures cristallines. *Acta Crystallogr 5*:802–810.

Mattevi A, Schierbeek AJ, Hol WGJ. 1991. Refined crystal structure of lipoamide dehydrogenase from *Azotobacter vinelandii* at 2.2 Å resolution. *J Mol Biol 220*:975–994.

Matthews BW. 1977. X-ray structure of proteins. In: Neurath H, Hill RL, eds. *The proteins, 3rd ed, vol 3*. New York: Academic Press. pp 403–590.

Meister A. 1989. A brief history of glutathione and a survey of its metabolism and functions. In: Dolphin A, Avramovic O, Poulson R, eds. *Coenzymes and cofactors, vol IIIA. Glutathione*. New York: Wiley. pp 1–48.

Mittl PRE, Berry A, Scrutton NS, Perham RN, Schulz GE. 1994. A designed mutant of the enzyme glutathione reductase from *Escherichia coli* shortens the crystallization time by a factor of forty. *Acta Crystallogr D 50*: 228–231.

Schiering N, Kabsch W, Moore MJ, Distefano MD, Walsh CT, Pai EF. 1991. Structure of the detoxification catalyst mercuric ion reductase from *Bacillus* sp. strain RC607. *Nature (Lond) 352*:168–172.

Schulz GE. 1980. Gene duplication in glutathione reductase. *J Mol Biol 138*:335–337.

Schulz GE. 1992. Binding of nucleotides by proteins. *Curr Opin Struct Biol 2*:61–67.

Scrutton NS, Berry A, Deonarain MP, Perham RN. 1990a. Active site complementation in engineered heterodimers of *Escherichia coli* glutathione reductase created in vivo. *Proc R Soc Lond B 242*:217–224.

Scrutton NS, Berry A, Perham RN. 1987. Purification and characterization of glutathione reductase encoded by a cloned and over-expressed gene in *Escherichia coli*. *Biochem J 245*:875–880.

Scrutton NS, Berry A, Perham RN. 1988. Engineering of an intersubunit disulphide bridge in glutathione reductase from *Escherichia coli*. *FEBS Lett 241*:46–50.

Scrutton NS, Berry A, Perham RN. 1990b. Redesign of a coenzyme specificity of a dehydrogenase by protein engineering. *Nature (Lond) 343*:38–43.

Scrutton NS, Deonarain MP, Berry A, Perham RN. 1992. Cooperativity induced by a single mutation at the subunit interface of a dimeric enzyme: Glutathione reductase. *Science 258*:1140–1143.

SERC Daresbury Laboratory. 1979. *Collaborative computing project no. 4. A suite of programs for protein crystallography*. Warrington, UK: SERC Daresbury Laboratory.

Sullivan FX, Sobolov SB, Bradley M, Walsh CT. 1991. Mutational analysis of parasite trypanothione reductase: Acquisition of glutathione reductase activity in a triple mutant. *Biochemistry 30*:2761–2767.

Tabor H, Tabor CW. 1975. Isolation, characterization, and turnover of glutathionyl-spermidine from *Escherichia coli*. *J Biol Chem 250*:2648–2654.